Available online at www.sciencedirect.com
ScienceDirect
Journal of the European Ceramic Society 28 (2008) 821–828
www.elsevier.com/locate/jeurceramsoc

Influence of cationic vacancies on the ionic conductivity of oxyapatites

P.J. Panteix [a,b,*], I. Julien [b], P. Abélard [b], D. Bernache-Assollant [c]

[a] *Centre Interuniversitaire de Recherche et d'Ingénierie des Matériaux, UMR 5085, Université Paul Sabatier, 118 Route de Narbonne, 31062 Toulouse Cedex 4, France*
[b] *Science des Procédés Céramiques et de Traitements de Surface, Université de Limoges, UMR 6638, 123 Avenue Albert Thomas, 87060 Limoges Cedex, France*
[c] *Ecole Nationale Supérieure des Mines, 158 Cours Fauriel, 42023 Saint-Etienne Cedex 2, France*

Received 2 May 2007; received in revised form 17 July 2007; accepted 27 July 2007
Available online 23 October 2007

Abstract

Oxyapatites are very promising materials in terms of ionic conductivity. They can be considered as a potential electrolyte for fuel cells as SOFC. Substituted silicated rare earth oxyapatites with formula $La_{9.33+z/3-x}Me_x\square_{0.67-z/3}(SiO_4)_6O_{2+z/2-x/2}$ ($z<x<z+4$) have been prepared by solid-state reaction at high temperature. Two series have been synthesized: a first one is oxygen stoichiometric with formula $La_{9.33-2x/3}Me_x\square_{0.67-x/3}(SiO_4)_6O_2$, and a second one is anion deficient with formula $La_{9.17-2x/3}Me_x\square_{0.83-x/3}(SiO_4)_6O_{1.75}\square_{0.25}$. In both cases, cationic vacancies are similarly controlled and vary from 0.67 to 0 per unit cell: the aim is to study the influence of cationic vacancies on the ionic conductivity with two distinct oxygen stoichiometries. Cell parameters of the high-purity oxyapatites have been refined in order to check the strontium incorporation. Discontinuous evolution of the *a* parameter underlined the strong electrostatic interactions between the defects of the most highly substituted samples. Electrical properties of the samples have also been studied by the complex impedance method between 280 and 620 °C. The evolution of conductivity and activation energy with the cationic vacancies content gives information on the conductivity mechanism, highlighting the importance of the global stoichiometry of the material.

Keywords: Powders solid-state reaction; Ionic conductivity; Apatite; Fuel cells

1. Introduction

The use of SOFC at intermediate temperatures (from 600 to 800 °C) is mainly limited by the electrolyte properties. One of the most important electrolytes is yttria-stabilized zirconia YSZ[1–4] which is well-known as an excellent oxygen-conducting electrolyte at temperatures beyond 1000 °C. Apatites seem to be very promising to be used as oxide ion conductors at intermediate temperatures. Indeed, the presence of large conduction channels containing oxide ions may suggest that materials with the apatite structure should be appropriate for such an application. A wide variety of materials crystallize in the hexagonal apatite structure (mineral formula $Me_{10}(XO_4)_6Y_2$, space group $P6_3/m$). Me represents a divalent cation, XO_4 a trivalent anion and Y a monovalent anion (Fig. 1). Me^{2+} cations are located in two different sites: four Me_I are at the centre of narrow tunnels (4f sites), six Me_{II} around large tunnels (6h sites) the centers of which are occupied by Y^- anions located on the hexad axis (2a sites). The coordination number of Me_I site is nine, whereas for Me_{II}, it is only seven.[5] A lot of substitutions can be observed in the apatite structure. Rare earth silicate oxyapatites such as $La_{9.33}\square_{0.67}(SiO_4)_6O_2$ seem to be very attractive in terms of oxide ions conductivity: oxide ions are located on the hexad axis in the centre of the large tunnels. As a consequence, oxyapatites are well-known as one-dimensional anionic conductors.[6–9]

Previous works have already reported the importance of the presence of cationic vacancies to explain the O^{2-} ions diffusion in the oxyapatite structure.[6,7] According to these studies, the existence of these unoccupied cationic sites allows a light displacement of O^{2-} ions in large tunnels: "interstitial-like" conduction paths are thus created, explaining the good conductivity values of these materials. These vacancies are supposed to be mainly located on Me_I sites.[10,14]

* Corresponding author at: Centre Interuniversitaire de Recherche et d'Ingénierie des Matériaux, UMR 5085, Université Paul Sabatier, 118 Route de Narbonne, 31062 Toulouse Cedex 4, France. Tel.: +33 5 61 55 61 20; fax: +33 5 61 55 61 63.
E-mail address: panteix@chimie.ups-tlse.fr (P.J. Panteix).

0955-2219/$ – see front matter © 2007 Elsevier Ltd. All rights reserved.
doi:10.1016/j.jeurceramsoc.2007.07.019

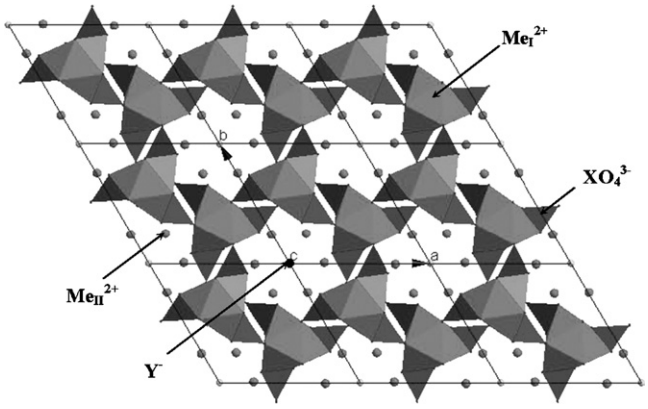

Fig. 1. View of hexagonal apatite structure $Me_{10}(XO_4)_6Y_2$.

A substantial increase in bulk conductivity by one to two orders of magnitude has been observed when the number of cationic vacancies is reduced[6]: Abram et al. have obtained the best results with alumina-substituted oxyapatites with the formula $La_{9.83}\square_{0.17}(SiO_4)_{4.5}(AlO_4)_{1.5}O_2$. The same kind of study is proposed here, yet with another way to control the number of cationic vacancies. Their number can be reduced by increasing the amount of La^{3+} per unit cell. The formulation of the corresponding oxyapatite can be expressed as: $La_{9.33+z/3}\square_{0.67-z/3}(SiO_4)_6O_{2+z/2}$, where z is the number of additional positive charges ($0<z<2$). As a consequence, the number of charge carriers (O^{2-}) also increases. In order to keep the oxide's stoichiometry, trivalent La^{3+} cations can be substituted by divalent cations Me^{2+}. The formulation thus becomes $La_{9.33+z/3-x}Me_x\square_{0.67-z/3}(SiO_4)_6O_{2+z/2-x/2}$, where x is the number of substituting Me^{2+} cations ($z<x<z+4$): with such substitutions, it is possible to control both cationic and anionic vacancies.

As a consequence, two series of oxyapatites with various cationic vacancies ratios have been prepared. In a first one, oxygen sites are fully occupied ($x=z$) with formulation $La_{9.33-2x/3}Me_x\square_{0.67-x/3}(SiO_4)_6O_2$: the amount of cationic vacancies varies from 0.67 to 0 per unit cell with $x=0$–0.5–1–1.5 and 2. Anion-deficient oxyapatites have also been synthesized: oxygen vacancies amount is fixed at 0.25 per unit cell ($z=x-1/2$) with formulation $La_{9.17-2x/3}Me_x\square_{0.83-x/3}(SiO_4)_6O_{1.75}\square_{0.25}$. Cationic vacancies also vary from 0.67 to 0 per unit cell with $x=0.5$–1–1.5–2 and 2.5. The divalent cation chosen for cationic substitutions was strontium Sr^{2+} which ionic radius (1.31 Å) is lightly higher than ionic radius of lanthanum La^{3+} (1.216 Å).[15] Ionic radii are given for CN = 9: indeed, for low substitution ratios, divalent cations are supposed to be mainly located in 4f sites (CN = 9) in oxyapatites structures.[7,11,16–22]

All the formulations are summarized in Table 1. The aim is to observe the influence of cationic vacancies on the electrical properties of oxyapatite materials with different stoichiometries of the charge carriers.

2. Materials and methods

2.1. Powder synthesis

Powders of La_2O_3 (Aldrich, 99.9%), SiO_2 (Prolabo, 99%), and $SrCO_3$ (Aldrich, 99.9%) were used as starting materials. Indeed, the use of divalent metal carbonates is suggested by many authors for the solid-state synthesis of substituted oxyapatites.[7,18,20,23–28] Weight losses of strontium carbonate and hygroscopic lanthanum oxide were determined before weighing by thermogravimetry, using the TA INSTRUMENTS SDT 2960. Appropriate amounts were mixed in ethanol and ground in a ball-mill (30 min, 180 rpm). The dried powders were then heated up to 1450 °C for 3 h, twice. An intermediate grinding was included between the two thermal treatments in order to improve the reactivity of the powders. Attrition has been performed for 1 h in ethanol at 490 rpm using a UNION PROCESS 01-Lab Attritor.

2.2. Densification

Samples were uniaxially pressed into discs (100 MPa) with green density about 55–60% of the theoretical value depending on the substitutions. Sintering was performed at 1550 °C for 3 h. Platinum sheets were used to support the pellets.

Table 1
Formulations and stoichiometries of the synthesized oxyapatites

	x	z	Formulation	Cationic vacancies/unit cell	Anionic vacancies/unit cell
Various cationic vacancies ratios 0 anionic vacancies/unit cell $La_{9.33-2x/3}Sr_x\square_{0.67-x/3}(SiO_4)_6O_2$	0	0	$La_{9.33}(SiO_4)_6O_2$	0.67	0
	0.5	0.5	$La_9Sr_{0.5}(SiO_4)_6O_2$	0.50	0
	1	1	$La_{8.67}Sr_1(SiO_4)_6O_2$	0.33	0
	1.5	1.5	$La_{8.33}Sr_{1.5}(SiO_4)_6O_2$	0.17	0
	2	2	$La_8Sr_2(SiO_4)_6O_2$	0	0
Various cationic vacancies ratios 0.25 anionic vacancies/unit cell $La_{9.17-2x/3}Sr_x\square_{0.83-x/3}(SiO_4)_6O_{1.75}\square_{0.25}$	0.5	0	$La_{8.83}Sr_{0.5}(SiO_4)_6O_{1.75}$	0.67	0.25
	1	0.5	$La_{8.5}Sr_1(SiO_4)_6O_{1.75}$	0.50	0.25
	1.5	1	$La_{8.17}Sr_{1.5}(SiO_4)_6O_{1.75}$	0.33	0.25
	2	1.5	$La_{7.83}Sr_2(SiO_4)_6O_{1.75}$	0.17	0.25
	2.5	2	$La_{7.5}Sr_{2.5}(SiO_4)_6O_{1.75}$	0	0.25

2.3. Characterizations

Powder X-ray diffraction (XRD) patterns were recorded with Cu Kα radiation in the 2θ range 17–120° on a $\theta/2\theta$ diffractometer (Siemens, Model D5000, Germany) (θ = diffraction angle). The crystalline phases were identified from a comparison of the registered patterns with the international center for diffraction data (ICDD) powder diffraction files (PDF).

Cell parameters were refined with the FULLPROF program.[29]

The relative densities of the sintered samples were obtained by Archimedes' method in water, using the calculated density determined by the measured cell parameters.

Electrical properties have been measured using a SOLARTRON 1260 Impedance/Gain Phase Analyzer. Measurements have been performed after both sides of the sintered disc were coated with Ag paste. The measurements have been made in the frequency range 1 Hz to 5 MHz at different temperatures rising from 280 to 620 °C. Complex impedance plots have been fitted with the software Z-live.[30]

3. Results and discussion

3.1. Synthesis

X-ray diffraction patterns of the prepared powders are presented in Figs. 2 (oxygen stoichiometric series) and 3 (0.25 oxygen vacancies per unit cell). In all cases, the main phase has an apatite structure. The lanthanum silicate $La_2Si_2O_7$ is also detected: the amount of this phase tends to decrease when the strontium content increases. Another lanthanum silicate, La_2SiO_5 is detected in both series when $x = 0.5$ Sr^{2+} per unit cell. Pure apatite phase is obtained when $x \geq 2$ for both series. As a consequence, it can be assumed that strontium incorporation tends to favor the formation of apatite more than the formation $La_2Si_2O_7$ and La_2SiO_5.

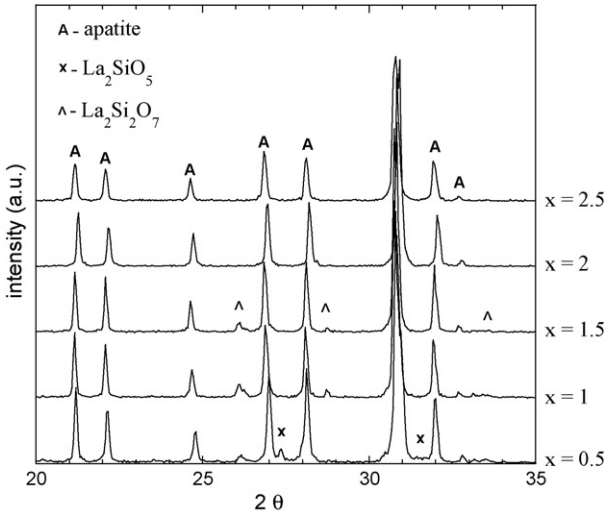

Fig. 3. X-ray diffraction patterns of synthesized $La_{9.17-2x/3}Sr_x(SiO_4)_6O_{1.75}$ powders.

It can be noticed that no secondary phase containing the strontium element has been detected, confirming the incorporation of Sr^{2+} in the apatite matrix. Indeed, some authors have observed the appearance of secondary phase as Me_2SiO_4 for high substitution ratios of divalent cations in an oxyapatite matrix.[28]

In order to determine the cell parameters of the sintered materials, the synthesized powders have been heated at 1550 °C for 3 h, i.e. the same conditions as those of the sintered samples. X-ray diffraction patterns of these samples are presented in Figs. 4 (oxygen stoichiometric samples) and 5 (0.25 oxygen vacancies per unit cell). The sintering thermal treatment caused the complete removal of the La_2SiO_5 phase (for $x = 0.5$ in both series), whereas $La_2Si_2O_7$ was not affected. Patterns of sample with stronger strontium substitution ratios ($x \geq 2$) still present pure apatite phases. Peaks are shifted towards larger and/or smaller diffraction angles: this confirms the dissolution

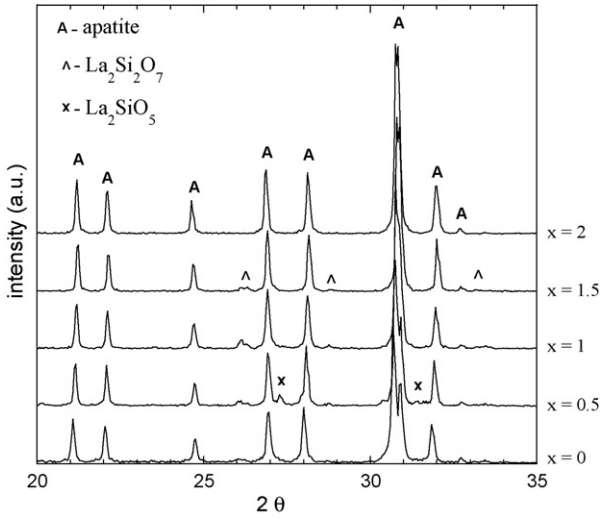

Fig. 2. X-ray diffraction patterns of synthesized $La_{9.33-2x/3}Sr_x(SiO_4)_6O_2$ powders.

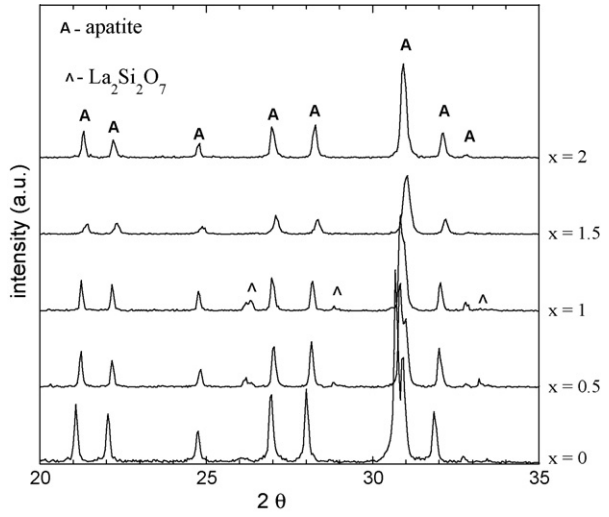

Fig. 4. X-ray diffraction patterns of $La_{9.33-2x/3}Sr_x(SiO_4)_6O_2$ powders after calcinations at 1550 °C for 3 h.

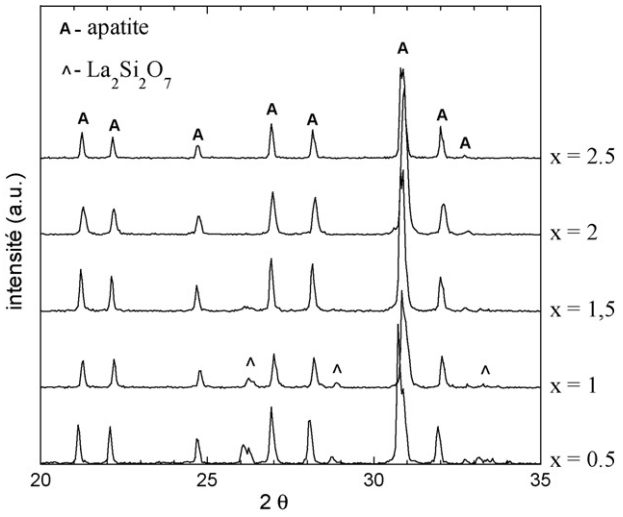

Fig. 5. X-ray diffraction patterns of $La_{9.17-2x/3}Sr_x(SiO_4)_6O_{1.75}$ powders after calcinations at 1550 °C for 3 h.

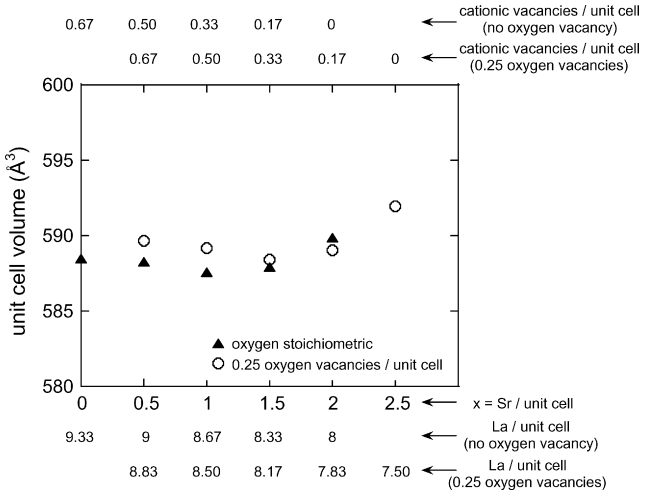

Fig. 6. Evolution of apatite cell volume: $La_{9.33-2x/3}Sr_x(SiO_4)_6O_2$ (no oxygen vacancy) and $La_{9.17-2x/3}Sr_x(SiO_4)_6O_{1.75}$ (0.25 oxygen vacancies).

of Sr^{2+} cations in the apatitic structure (Sr^{2+} has an ionic radius lightly greater than La^{3+}).

Cell parameters of all the compounds have been refined by a whole pattern fitting method. A good agreement has been obtained between observed and calculated spectra with R Bragg factors comprised between 2.38 and 4.07. The presence of $La_2Si_2O_7$ has been taken into account for $x = 0$–0.5 and 1 (oxygen stoichiometric samples) and for $x = 0.5$ and 1 (0.25 oxygen vacancies per unit cell). The evolution of the unit cell volume with Sr content, La content and cationic vacancies content is presented in Fig. 6 for both series. They both present similar evolutions. Unit cell volume remains constant for low strontium substitution rates ($x \leq 1.5$), despite the increase of cations content ($La^{3+} + Sr^{2+}$). Unit cell volume then suddenly increases for higher strontium contents ($x > 1.5$). The evolution of *a* and *c* cell parameters of hexagonal apatite can explain such a behavior (Fig. 7). The *c* parameters steadily increases with the strontium insertion, whereas the *a* parameter first decreases and then suddenly increases when $x > 1.5$. The same kind of results have been obtained by Sansom et al. who studied strontium-substituted oxyapatites with formula $La_{9.33-2x/3}Sr_xSi_6O_{26}$.

According to the theoretical formulation ($La_{9.33+z/3-x}Me_x\square_{0.67-z/3}(SiO_4)_6O_{2+z/2-x/2}\square_{x/2-z/2}$) one Sr^{2+} ion replaces 0.66 La^{3+} ions and 0.33 cationic vacancies: globally, the number of cations per unit cell increases with the insertion of Sr^{2+} ions. As a consequence, the increase observed in the *c* parameter is logical. On the other hand, the evolution of the *a* parameter is more unexpected. The X-ray diffraction patterns used for the cell parameters refinements show that apatite phases are relatively pure (Figs. 4 and 5), without any secondary phase containing strontium: this one is totally inserted in the apatite matrix, and the unexpected evolutions of the cell parameters are thus not ascribable to a random insertion of strontium in apatite or to significant variations of real stoichiometry compared to theoretical stoichiometry. It is thus extremely probable that the evolutions observed in Figs. 6 and 7 are above all due to electrostatic interactions between the various defects found in the apatite cell:

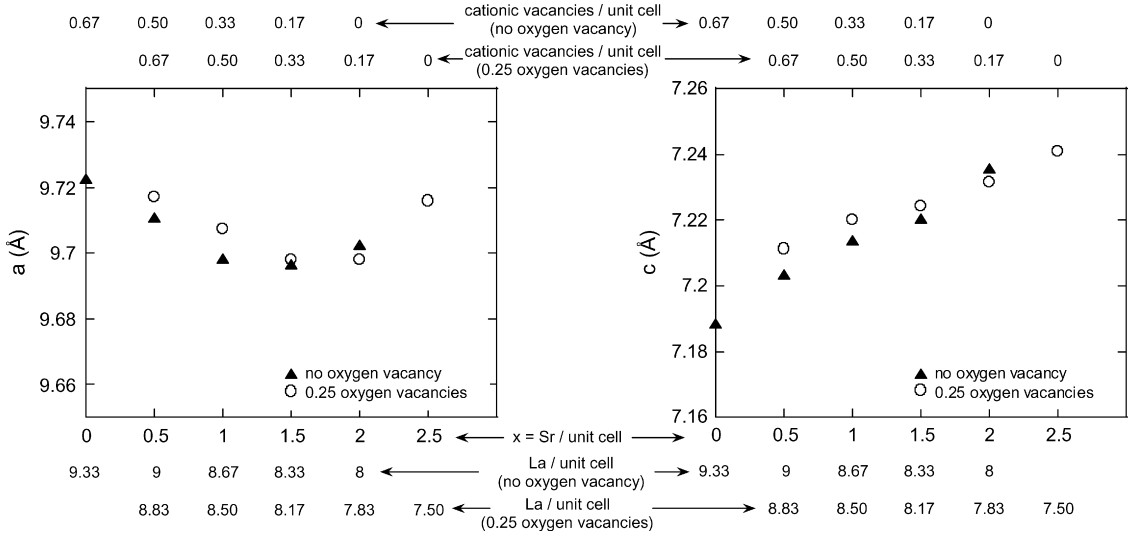

Fig. 7. Evolution of *a* and *c* cell parameters: $La_{9.33-2x/3}Sr_x(SiO_4)_6O_2$ (no oxygen vacancy) and $La_{9.17-2x/3}Sr_x(SiO_4)_6O_{1.75}$ (0.25 oxygen vacancies).

the effects due to the insertion of a cation lightly larger than lanthanum would thus be supplanted by these interactions. The defects varying from one composition to another are as follows:

- cationic vacancies (negatively charged);
- anionic vacancies (positively charged);
- divalent cations in the place of trivalent cations (negatively charged).

The anionic vacancies in all the cases are located in the tunnels of the type II (2a sites). The cationic vacancies and the divalent cations can be located in the tunnels of the type I (4f sites) or at the periphery of the tunnels of the type II (6h sites). The literature suggests that these two types of defects are preferentially located in 4f sites for low substitution rates.[10–14,16–22] However, it can be supposed that their repartition evolves with the extent of substitution: a certain number of these defects may come in 6h sites when the rate of substitution increases. A complete refinement of the structure of all apatites of the two series could bring further information on the evolutions of the cell parameters observed here. However, the regular increase of the *c* parameter indicates that the insertion of strontium is regularly achieved in the apatite matrix.

Densification ratios of all the sintered pellets are all greater than 90%: as a consequence, the influence of porosity on the electrical properties of the bulk material can be neglected.

3.2. Electrical properties

Complex impedance plots (Z'' vs. Z') consisted of two overlapping arcs and a low frequency contribution with an associated capacitance of a few μF. A typical example of complex impedance plot is shown in Fig. 8 in a Nyquist format for the $La_{8.17}Sr_{1.5}\square_{0.33}(SiO_4)_6O_{1.75}\square_{0.25}$ apatite at 500 °C. The low frequency contribution is attributed to ionic polarization and diffusion-limited phenomena at the Ag electrode. The first semi-circle in the high frequency region corresponds to the bulk component, whereas the other, in the intermediate frequency region corresponds to the grain boundaries contribution. The bulk components were considered in order to determine the conductivity values noted σ. These values were calculated with the formula $\sigma = t/(RS)$, where R is the bulk resistance, t and S the samples thickness and area, respectively. R was extracted from the intercept of the high frequency arc with the real Z' axis after refinement of the complex impedance spectra. The associated capacitances of the high frequency arcs were calculated to be a few pF using the relationship $\omega RC = 1$ at Z'_{max} (where ω is the angular frequency and $\omega = 2\pi f$, where f is the applied frequency), which is consistent with the bulk response. The associated capacitances of the mid-frequency arcs were calculated to be a few nF, which is consistent with their assignment to the grain boundaries response.

Globally, the samples impedance decreases when the temperature increases. Refined bulk conductivity data of all samples are shown in an Arrhenius representation in Fig. 9 (oxygen stoichiometric oxyapatites (a) and oxygen-deficient oxyapatite (b)). The data were parameterized by the Arrhenius equation $\sigma = \sigma_0 \exp(-\Delta E_a/kT)$, where σ, σ_0, ΔE_a, k and T are the conductivity, pre-exponential factor, activation energy, Boltzmann constant and absolute temperature, respectively. The temperature dependence on samples containing 0 cationic vacancy per unit for $La_{9.33-2x/3}Sr_x(SiO_4)_6O_2$ apatites, $La_{9.17-2x/3}Sr_x(SiO_4)_6O_{1.75}$ and 0.17 and 0 cationic vacancies per unit cell for $La_{9.17-2x/3}Sr_x(SiO_4)_6O_{1.75}$ apatites are not presented: the impedances of these samples were too high to be measured, and furthermore to be refined.

In order to get accurate results, conductivities have been determined at 500 °C ($1000/T \sim -271.85\,°C^{-1}$): the best impedance plots refinements have been obtained at this temperature with limited electrode contribution and well-defined high frequency semi-circles (Fig. 8). Activation energies have been calculated from the linear fitting of the conductivity data measured between 300 and 600 °C: the best refinements of bulk conductivity values have been obtained in this temperature range. The evolutions of bulk conductivities at 500 °C and activation energies are presented in Fig. 10(a) (oxygen stoichiometric apatites) and in Fig. 11 (oxyapatites with 0.25 oxygen vacancies per unit cell). The results of the oxygen stoichiometric apatites (Fig. 10(a)) can be compared to those obtained by Abram et al.[6] on alumina-substituted oxyapatites with formula $La_{9.83}\square_{0.17}(SiO_4)_{4.5}(AlO_4)_{1.5}O_2$ (Fig. 10(b)): cationic vacancies ratios variations are the same as for the oxyapatites synthesized here. In both cases, a decrease of the cationic vacancies content involves a significant increase of the ionic conductivity (one half order of magnitude for the strontium-substituted oxyapatites, and two orders of magni-

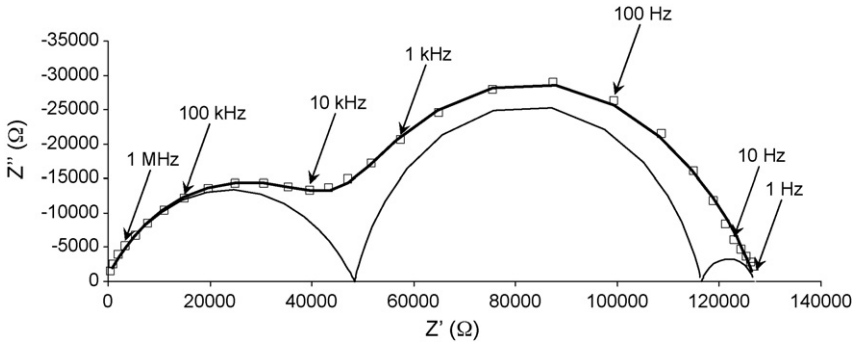

Fig. 8. Complex impedance plot at 500 °C of $La_{8.17}Sr_{1.5}\square_{0.33}(SiO_4)_6O_{1.75}\square_{0.25}$.

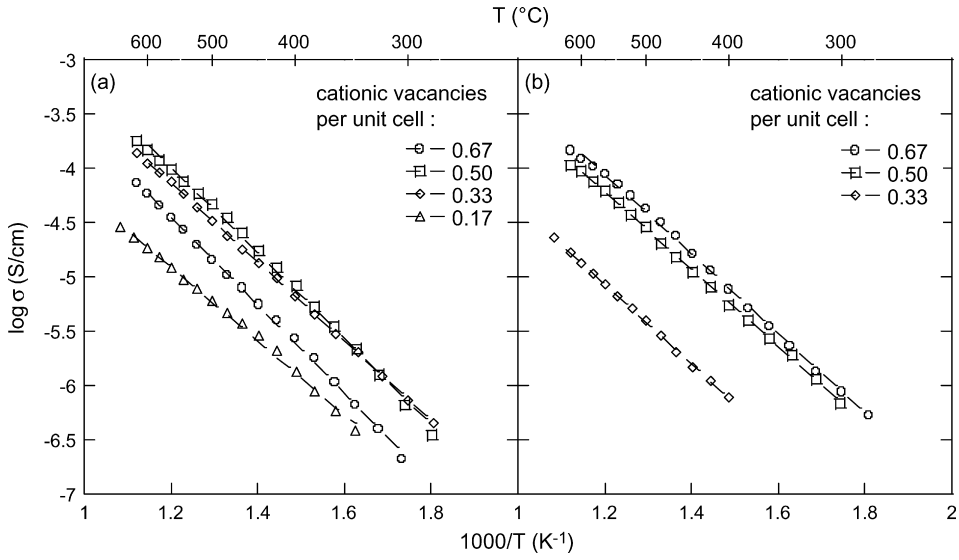

Fig. 9. Temperature dependence on bulk conductivity of $La_{9.33-2x/3}Sr_x(SiO_4)_6O_2$ (a) and $La_{9.17-2x/3}Sr_x(SiO_4)_6O_{1.75}$ (b).

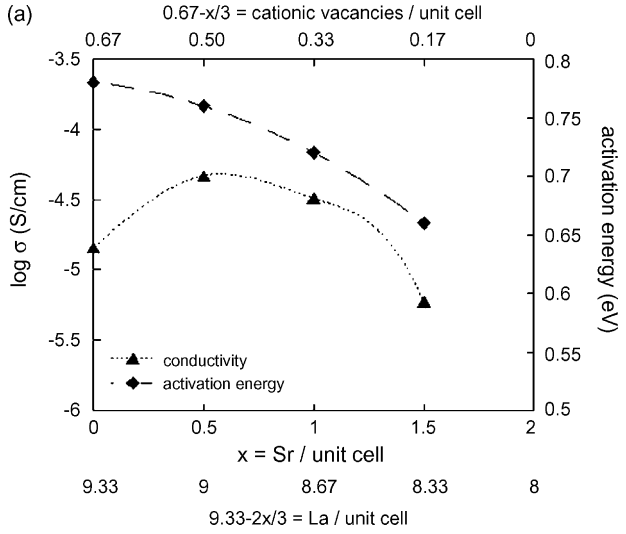

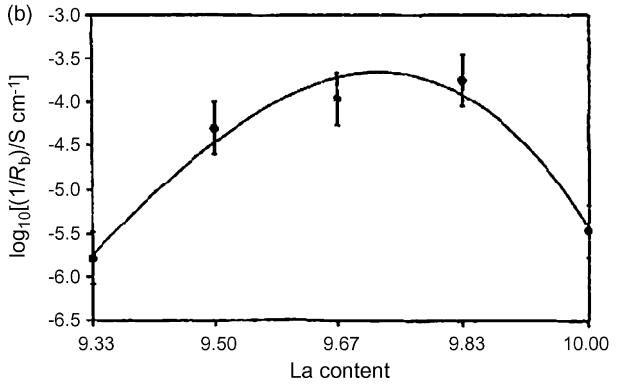

Fig. 10. (a) Evolution of the bulk conductivity and of activation energy at 500 °C of $La_{9.33-2x/3}Sr_x(SiO_4)_6O_2$ apatites with Sr content, La content and cationic vacancies content; (b) variation of bulk conductivity with La content at ~300 °C for Al-doped $La_{9.33}(SiO_4)_6O_2$.[7]

tude for AlO_4-substituted oxyapatites). A maximum is reached before a decrease. This maximum is not the same for both series: it is comprised between 0.50 and 0.33 cationic vacancies per unit cell for strontium-substituted oxyapatites, and it is around 0.17 cationic vacancies per unit cells for AlO_4-substituted oxyapatites.[7] Furthermore, the conductivity decrease is much faster for strontium oxyapatites than for AlO_4-substituted ones: it is not measurable for strontium samples without any cationic vacancy, whereas it goes back to unsubstituted oxyapatites conductivity values for Abram's samples. The same kind of electrical behavior has been observed by Arikawa et al. for Sr-doped oxyapatites with formula $La_{10-x}Sr_xSi_6O_{27-2x/3}$[32] (the best conductivity value is measured when $x = 0.25$) and by Sansom et al. for oxyapatites with formula $La_{9.33-2x/3}Sr_xSi_6O_{26}$ (the conductivity of samples highly doped with Sr decrease[31]). A continuous decrease is observed for strontium samples contain-

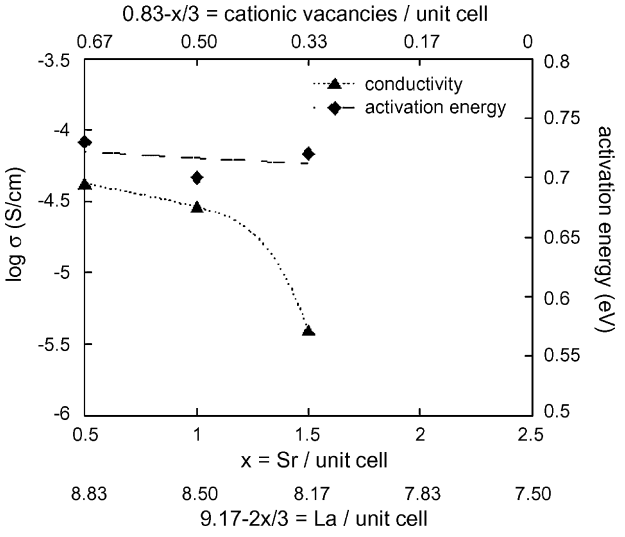

Fig. 11. Evolution of the bulk conductivity and of activation energy at 500 °C of $La_{9.17-2x/3}Sr_x(SiO_4)_6O_{1.75}$ apatites with Sr content, La content and cationic vacancies content.

ing 0.25 oxygen vacancies per unit cell (Fig. 11). The activation energy regularly decreases in Fig. 10(a) and remains constant in Fig. 11, even when the conductivity decreases, which is a very surprising result. This point is not consistent with previous work reported by Sansom et al.[31] where the activation energy tends to increase with the Sr incorporation in oxyapatites with formula $La_{9.33-2x/3}Sr_xSi_6O_{26}$.

Earlier studies have already shown the importance of the presence of cationic vacancies located in 4f sites (type I tunnels)[6,33]: crystal structure refinements showed that the presence of these vacancies allows for a displacement (a few 0.1 Å) of SiO_4 tetrahedra. As a consequence, some O^{2-} ions located in 2a sites (14% in $La_{9.33}(SiO_4)_6O_2$) might be displaced to "interstitial-like" positions, creating "Frenkel-like" defects. These particular positions might be the cause of the O^{2-} ions conduction process, even if the way of diffusion has not been exactly defined yet. As a consequence, the rough decrease of conductivity of both strontium-substituted oxyapatites series can be explained by the lack of cationic vacancies allowing good diffusion paths through large tunnels.

Furthermore, the evolutions of the conductivity can be correlated to the evolutions of the cell parameters of the substituted oxyapatites described above. Figs. 12 and 13 show the superposition of these two evolutions for both series. It is interesting to notice that the conductivity decreases when the evolution of the apatites cell volume present discontinuity. The strong electrostatic interactions between defects of highly substituted oxyapatites which are supposed to cause the discontinuous evolution of cell parameters might also explain the rough decrease of conductivity: these interactions might limit the diffusion of some charge carriers.

As a consequence, this might also explain the evolution of activation energy, which decreases even when the conductivity decreases. Indeed, the activation energy is inversely proportional to the conducting ions' mobility ($E_a \sim \ln(1/\mu)$), whereas the conductivity is proportional to both mobile species concentration and mobility ($\sigma \sim C\mu$). The evolutions observed for highly substituted samples can thus be explained by a decrease of the mobile ions concentration (explaining the decrease of conductivity), while the mobility of the ions still moving through the crystal structure is improved by the electrostatic interactions: this may explain the continuous decrease of activation energy. However, the conduction process in these materials seems to be very complex and very dependent on the global stoichiometry. Too great an amount of punctual defect may highly limit the oxide ions diffusion.

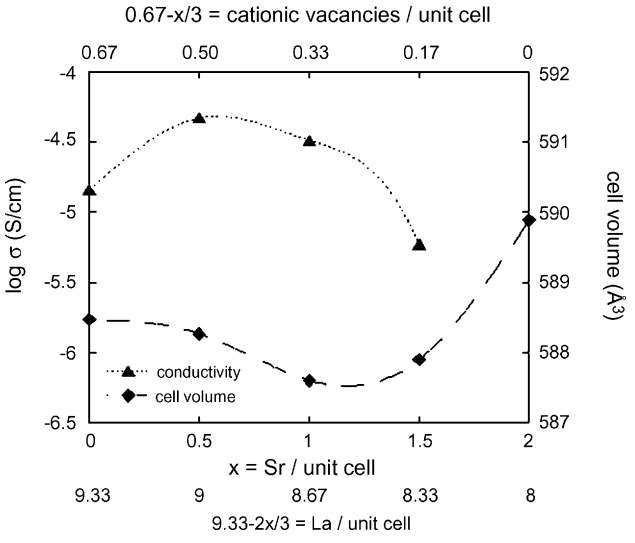

Fig. 12. Evolution of the bulk conductivity at 500 °C and of cell volume of $La_{9.33-2x/3}Sr_x(SiO_4)_6O_2$ apatites with Sr content, La content and cationic vacancies content.

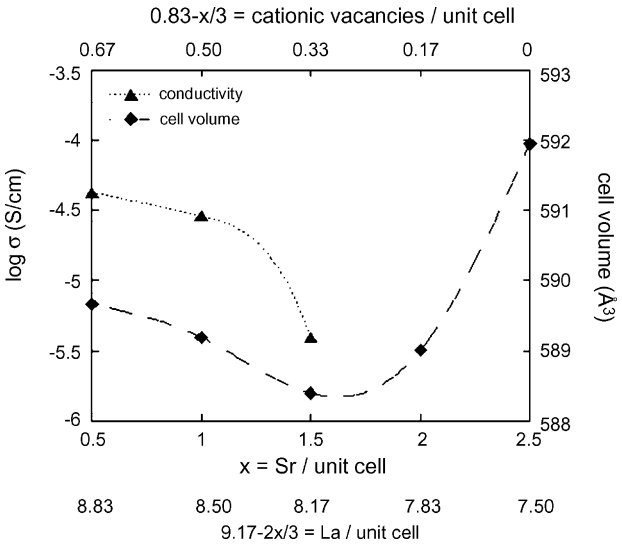

Fig. 13. Evolution of the bulk conductivity at 500 °C and of cell volume of $La_{9.17-2x/3}Sr_x(SiO_4)_6O_{1.75}$ apatites with Sr content, La content and cationic vacancies content.

4. Conclusion

Substituted anion conductors with formula $La_{9.33+z/3-x}Sr_x\square_{0.67-z/3}(SiO_4)_6O_{2+z/2-x/2}$ (with $z<x<z+4$) have been successfully prepared by solid-state synthesis at high temperature. Based on this formulation, it is possible to control the stoichiometry of two kinds of punctual defects: cationic vacancies and oxide ions vacancies. Two series have been prepared. A first one is oxygen stoichiometric with formula $La_{9.33-2x/3}Sr_x\square_{0.67-x/3}(SiO_4)_6O_2$, and a second contains 0.25 oxide ions vacancies per unit cell with formula $La_{9.17-2x/3}Sr_x\square_{0.83-x/3}(SiO_4)_6O_{1.75}\square_{0.25}$. In both series, cationic vacancies ratio varied from 0.67 to 0 per unit cell. High-purity apatite phases have been obtained, especially for the higher substitutions ratios. Cell parameters refinement gave information on the strontium incorporation in the apatite structure: in both cases, cell volume remains constant for lower substitution rates ($x<1.5$) and then suddenly increases. Indeed, the *c* parameter regularly increases (attesting to a good incorporation of strontium in the apatite matrix), but the *a* parameter first decreases before a discontinuous increase for higher substitution ratios. This phenomenon has been attributed to electrostatic interactions between the various defects introduced in the highly substituted samples.

Electrical properties of the samples have been studied. Refinement of the complex impedance plots gave the bulk conductivity values at 500 °C and the activation energy of the conduction process. An improvement of the conductivity about one half order of magnitude is observed for low substitution rates for the oxygen stoichiometric samples, with a simultaneous decrease of activation energy. Higher substitution ratios tend to lower the conductivity, with a surprisingly still decreasing activation energy. The conductivity of apatites with vacancies of charge carriers decreases continuously, with a rougher decrease for higher substitution ratios. These results highlight the importance of cationic vacancies for the oxide ions diffusion: their presence in 4f sites might involve the creation of particular pathways in the conduction tunnels. Furthermore, the rough decrease of the conductivity of highly substituted apatites has been correlated to the discontinuous evolution of cell parameters: electrostatic interactions between punctual defects causing increasing of the *a* parameter should also be responsible for the limited oxide ions diffusion. The continuous decrease of activation energy has also been attributed to these electrostatic interactions. These interactions might improve the mobility of the ions which are still diffusing. As a consequence, the great complexity of the O^{2-} conduction in oxyapatites has been underlined, showing that their displacements might be strongly dependent on the global stoichiometry of the materials.

References

1. Yamamoto, O., Solid oxide fuel cell: fundamental aspects and prospects. *Electrochim. Acta*, 2000, **45**, 2423–2435.
2. Minh, N. Q. and Takahashi, T., *Science and Technology of Ceramic Fuel Cells*. Elsevier, 1995.
3. Minh, N. Q., Ceramic fuel cells. *J. Am. Ceram. Soc.*, 1993, **76**(3), 563–588.
4. Chen, X. J., Khor, K. A., Chan, S. H. and Yu, L. G., Influence of microstructure on the ionic conductivity of yttria-stabilized zirconia electrolyte. *Mater. Sci. Eng. A*, 2002, **335**, 246–252.
5. Elliott, J. C., Structure and chemistry of the apatites and other calcium orthophosphates. *Elsevier*, 1994.
6. Abram, E. J., Sinclair, D. C. and West, A. R., A novel enhancement of ionic conductivity in the cation-deficient apatite $La_{9.33}(SiO_4)_6O_2$. *J. Mater. Chem.*, 2001, **11**, 1978–1979.
7. Sansom, J. E. H., Riching, D. and Slater, P. R., A powder neutron diffraction study of the oxide-ion-conducting apatite-type phase, $La_{9.33}Si_6O_{26}$ and $La_8Sr_2Si_6O_{26}$. *Solid State Ionics*, 2001, **139**, 205–210.
8. Takahashi, M., Uematsu, K., Ye, Z. E. and Sato, M., Single-crystal growth and structure determination of a new oxide apatite, $NaLa_9(GeO_4)_6O_2$. *J. Solid State Chem.*, 1998, **139**, 304–309.
9. Nakayama, S., Sakamoto, M., Higuchi, M., Kodaira, K., Sato, M., Kakita, S. *et al.*, Oxide ionic conductivity of apatite type $Nd_{9.33}(SiO_4)_6O_2$ single crystal. *J. Eur. Ceram. Soc.*, 1999, **19**, 507–510.
10. Felsche, J., Rare earth silicates with the apatite structure. *J. Solid State Chem.*, 1972, **5**, 266–275.
11. Berastegui, P., Hull, S., Garcia Garcia, F. J. and Grins, J., A structural investigation of $La_2(GeO_4)O$ and alkaline-earth-doped $La_{9.33}(GeO_4)_6O_2$. *J. Solid State Chem.*, 2002, **168**, 294–305.
12. Bernache-Assollant, D., Ababou, A., Champion, E. and Heughebaert, M., Sintering of calcium phosphate hydroxyapatite $Ca_{10}(PO_4)_6(OH)_2$. I. Calcination and particle growth. *J. Eur. Ceram. Soc.*, 2003, **23**, 229–241.
13. Leon-Reina, L., Losilla, E. R., Martinez-Lara, M., Bruque, S. and Aranda, M. A. G., Interstitial oxygen conduction in lanthanum oxy-apatite. *J. Mater. Chem.*, 2004, **14**, 1142–1149.
14. Sansom, J. E. H. and Slater, P. R., Oxide ion conductivity in the mixed Si/Ge apatite-type phases $La_{9.33}Si_{6-x}Ge_xO_{26}$. *Solid State Ionics*, 2004, **167**, 23–27.
15. Shannon, R. D., Revised effective ionic radii and systematic studies of interatomic distances in halides and chalcogenides. *Acta Crystallogr. A*, 1976, **32**, 751–767.
16. Schroeder, L. W. and Mathew, M., Cation ordering in $Ca_2La_8(SiO_4)_6O_2$. *J. Solid State Chem.*, 1978, **26**, 383–387.
17. Fahey, J. A. and Weber, A., The crystal structure and stoichiometry of the $Ca_{2+x}Nd_{8-x}(SiO_4)_6O_{2-0.5x}$ system. *The Rare Earths in Modern Science and Technology*, *vol. 3*. Plenum Publishing Corporation, 1982, pp. 341–344.
18. Benmoussa, H., Mikou, M., Lacout, J. L. and Synthesis, Physicochemical study of new rare-earth-containing vanado calcic oxyapatites. *Mater. Res. Bull.*, 1999, **34**(9), 1429–1434.
19. Benmoussa, H., Mikou, M., Bensaoud, A., Bouhaouss, A. and Morineaux, R., Electrical properties of lanthanum containing vanadocalcic oxyapatite. *Mater. Res. Bull.*, 2000, **35**, 369–375.
20. Serret, A., Cabanas, M. V. and Vallet-Regi, M., Stabilization of calcium oxyapatites with lanthanum(III)-created anionic vacancies. *Chem. Mater.*, 2000, **12**, 3836–3841.
21. Bouhaouss, A., Laghzizil, A., Bensaoud, A., Ferhat, M., Lorent, G. and Livage, J., Mechanism of ionic conduction in oxy and hydroxyapatite structure. *Int. J. Inorg. Mater.*, 2001, **3**, 743–747.
22. Carpena, J., Boyer, L., Fialin, M., Kienast, J. R. and Lacout, J. L., Ca^{2+}, $PO_4^{3-} = Ln^{3+}$, SiO_4^{4-} coupled substitution in the apatite structure: stability of the mono-silicated fluor-britholite. *Earth Planet. Sci.*, 2001, **333**, 373–379.
23. Slater, P. R., Irvine, J. T. S., Ishihara, T. and Takita, Y., The structure of the oxide ion conductor $La_{0.9}Sr_{0.1}Ga_{0.8}Mg_{0.2}O_{2.85}$ by powder neutron diffraction. *Solid State Ionics*, 1998, **107**, 319–323.
24. Takeda, H., Ohgaki, M., Kizuki, T., Hashimoto, K., Toda, Y., Udagawa, S. *et al.*, Formation mechanism and synthesis of apatite-type structure $Ba_{2+x}La_{8-x}(SiO_4)_6O_{2-\delta}$. *J. Am. Ceram. Soc.*, 2000, **83**(11), 2884–2886.
25. Zhang, X., Ohara, S., Okawa, H., Maric, R. and Fukui, T., Interaction of $La_{0.9}Sr_{0.1}Ga_{0.8}Mg_{0.2}O_{3-\delta}$ electrolyte with Fe_2O_3, Co_2O_3 and NiO anode materials. *Solid State Ionics*, 2001, **139**, 145–152.
26. Naddari, T., Synthèse, *Structure Et Propriétiés Des Apatites Lacunaires: Une Option Pour Le Piégeage Du Plomb*. PhD thesis, L'Université de Sud, Faculté des Sciences de Sfax, 2002.
27. Skellern, M. G. and Skakle, J. M. S., Subsolidus relations in the $BaO–La_2O_3–V_2O_5$ phase diagram. *J. Eur. Ceram. Soc.*, 2002, **22**, 2933–2937.
28. Kizuki, T., Ohgaki, M., Nakamura, T., Hashimoto, K., Toda, K. and Yamashita, K., *Synthesis of New Biocompatible Apatite-type Rare-earth Silicates. Conference Bioceramics*, *vol. 15*. Trans. Tech. Publication, Sydney, 2003, pp. 559–562.
29. Rodriguez-Carvajal, J., FULLPROF Program, see http://www-llb.cea.fr/fullweb/fp2k/fp2k.html.
30. Georges, S., Zlive Program, see www.univ-lemans.fr/sciences/fluorures/ldf.html.
31. Sansom, J. E. H., Kendrick, E., Tolchard, J. R., Islam, M. S. and Slater, P. R., A comparison of the effect of rare earth vs. Si site doping on the conductivities of apatite-type rare earth silicates. *J. Solid State Electrochem.*, 2006, **10**, 562–568.
32. Arikawa, A., Nishiguchi, H., Ishihara, T. and Takita, Y., Oxide ion conductivity in Sr-doped $La_{10}Ge_6O_{27}$ apatite oxide. *Solid State Ionics*, 2000, **136/137**, 31–37.
33. Tolchard, J. R., Islam, M. S. and Slater, P. R., Defect chemistry and oxygen ion migration in the apatite-type materials $La_{9.33}Si_6O_{26}$ and $La_8Sr_2Si_6O_{26}$. *J. Mater. Chem.*, 2003, **13**, 1956-1561.